ADVANCED OPTICAL MATERIALS
www.advopticalmat.de

Pathways of Exciton Triggered Hot-Carrier Injection at Plasmonic Metal–Transition Metal Dichalcogenide Interface

Xiewen Wen, Weipeng Wang, Xiang Zhang, Hailong Chen, Shuai Jia, Yongji Gong, Weibing Chen, Yanfeng Wang, Hanyu Zhu, Junrong Zheng, P. M. Ajayan,* and Jun Lou**

Surface plasmon induced hot-carrier injection to semiconducting transition metal dichalcogenide (TMD) monolayers has been extensively studied. However, comprehensive understanding of the injection kinetics by fully considering the weak metal–TMD interaction and the TMDs' exciton formation kinetics is missing. Here, a hot-carrier injection pathway is elucidated by systematically investigating the interfacial interaction kinetics among different plasmonic metals and TMDs. The pathway highlights the exciton formation timescale as a threshold for interfacial carrier injection, before which plasmonic hot carriers and free electron–hole pairs are relaxed incoherently across the interface. The injected hot carriers will interact with excitons to form charged quasiparticles as trions, which have extended lifetime. The pathway reveals the fundamental mechanism of the plasmonic hot-carrier–TMD interactions, opens the possibility of controllable manipulation of hot-carrier injection process, and allows future research toward opto-electrical guidance of trions in metal–TMD systems.

1. Introduction

Surface plasmon resonance (SPR) induced light-matter interaction has drawn considerable research attention from both fundamental and practical aspects. The SPR has been extensively used to improve the quantum efficiency of photocatalysis, photovoltaics, and photodetectors.[1] Different interaction mechanisms of SPR-matter interaction such as local field enhancement,[2] hot-carrier generation/injection,[3] and plasmon-exciton coupling[4] are proposed, understanding the fundamental mechanism behind them can inspire new device applications. Among the SPR-semiconductor interaction mechanisms studied, the existence and the pathway of the hot-carrier interaction process are intricate in different systems, with various models proposed. As schematically illustrated in **Figure 1**, researchers have proposed different mechanisms of SPR induced hot-carrier transfer, e.g., hot-electrons produced by Landau damping directly transfer to the conduction band of semiconductors in Figure 1a, and direct optical excitation of hot electrons from metal into the conduction band of the semiconductor as in Figure 1b. The former one follows the traditional hot-carrier injection process[5] while the latter one is based on coherent interfacial interaction.[6,7]

With the emergence of transition metal dichalcogenides (TMDs) monolayers, featuring a direct band gap as well as a large exciton binding energy that make them perfect candidates to study the surface plasmon–semiconductor interaction. The SPR approach has been proven to be efficient to tune and to enhance the TMD-based optoelectrical[8,9], photovoltaic,[10] photoelectrochemical,[11] Raman,[12,13] and nonlinear optical devices.[14] Although common understanding as well as successful tuning of the local field enhancement and plasmon-exciton interactions have been demonstrated, the dynamics of hot-carrier injection process in plasmonic nanoparticle-TMDs have remained elusive both experimentally and theoretically. Regarding to the dynamic hot-carrier interaction process in SPR-TMD systems, two major puzzles are to be solved, i.e., the existence of the hot-carrier injection process and the corresponding pathway for the injection process, as the crystalline structure of the TMD monolayers has dictated unique dynamic processes and underlying mechanisms of pristine TMDs upon SPR-TMD interactions. The saturated surface of TMD family possesses weak van der Waals interactions with plasmonic metals,[15,16]which may hinder the hot-carrier injection process as the subsistent injection mechanism is mainly

X. Wen, W. Wang, X. Zhang, S. Jia, Y. Gong, W. Chen, H. Zhu, P. M. Ajayan, J. Lou
Department of Materials Science and NanoEngineering
Rice University
6100 Main Street, Houston, TX 77005, USA
E-mail: wpwang@mail.tsinghua.edu.cn; ajayan@rice.edu; jlou@rice.edu

W. Wang, Y. Wang
Key Lab of Advanced Materials (MOE)
School of Materials Science and Engineering
Tsinghua University
Beijing 100084, China

H. Chen
Beijing National Laboratory for Condensed Matter Physics
CAS Key Laboratory of Soft Matter Physics
Institute of Physics
Chinese Academy of Sciences
Beijing 100190, China

J. Zheng
College of Chemistry and Molecular Engineering
Beijing National Laboratory for Molecular Sciences
Peking University
Beijing 100871, China

The ORCID identification number(s) for the author(s) of this article can be found under https://doi.org/10.1002/adom.202100070.

DOI: 10.1002/adom.202100070

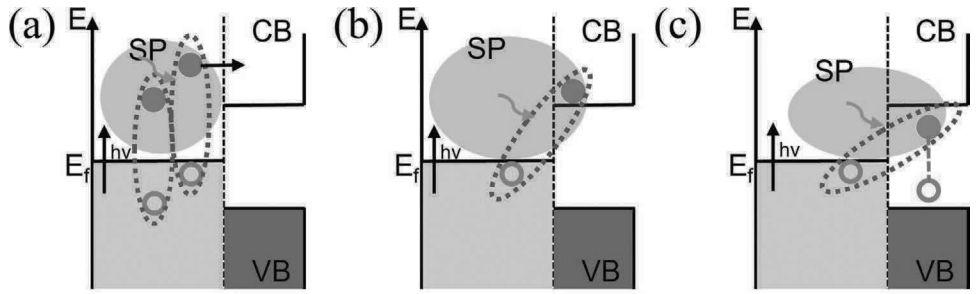

Figure 1. Possible interaction process at the plasmonic metal–semiconductor interface. a) Plasmonic hot-carrier injection to the conduction band of semiconductors. The pathway was described as traditional interaction mechanism, with surface plasmons damped to hot carriers and injected to semiconductor conduction band by overcoming the Schottky barrier. b) Direct optical excitation of hot carriers from metal into the conduction band of the semiconductor. The foundation of this phenomenon is coherent interfacial interaction between the plasmonic metal and the semiconductors. c) Possible carrier injection pathway of surface plasmon resonance (SPR) transition metal dichalcogenide (TMD) interactions. SPR induced hot-carrier transfer to the excitonic bands of TMDs, interacting with the as-formed excitons to form complex quasiparticles.

interface interaction dependent (Figure 1a,b). Moreover, due to the suppression of Coulomb screening, the exciton binding energy of TMD monolayers is very large,[17] enabling room temperature exciton formation. The exciton formation time of the TMDs is reported to be in the range of 100–500 fs,[18] similar to the plasmonic hot-carrier relaxation timescale.[19]The timescale overlapping as well as the weak interactions suggest a thorough examination of the SPR-TMD dynamic interactions by distinguishing individual processes from each other is critically needed, as none of the proposed models are believed to cover the SPR-TMD interaction processes by fully considering the weak metal-TMD interaction and the TMD exciton formation process. Moreover, existing models normally take the conduction band of semiconductors as hot-carrier acceptor, with little efforts to describe the hot carrier-exciton interaction (Figure 1c).

The absence of a comprehensive understanding of the plasmonic carrier interaction with TMDs thus inspire us to consider the scenario that in addition to the universal existence of the local field enhancement effects by the plasmonic metals, the hot-carrier interaction process might involve new mechanism during the light-matter interaction process. However, both puzzles are challenging to be solved by the absorption, photoluminescence, or photocurrent measurements, as the aforementioned steady-state methods can only observe the absolute change of light absorption, emission, and/or photocurrent intensities while being incapable to distinguish the contribution between local field enhancement and hot-carrier transfer.[3] Dynamical optical techniques based on time-resolved characterizations of the light-matter interactions, e.g. time-dependent luminescence, photoelectron emission,[20–22] and ultrafast pump-probe spectroscopy,[23] are thus believed to be more suitable to study the kinetics and to differentiate the contributions by emphasizing charge/energy transfer process.[23–25]

Recently, there have been numerous experimental efforts on the dynamics of exciton-plasmon coupling in 2D semiconductor/metal nanostructures,[26–28] we hereby provide a comprehensive dynamic observation of plasmonic hot-carrier injection pathway in the plasmonic metal-MoX_2 system. MoS_2 and $MoSe_2$ monolayers were selected given their highly crystalline structures and same ground state excitons and band polarity, while possessing different band structures and phonon-induced dynamic processes.[17]On the other hand, silver and gold nanoparticles were chosen as they both demonstrated extensively studied plasmonic enhancement effects over bulk metals, with varying resonance peak positions, vacuum Fermi levels, local enhancements as well as the photodynamic processes.[19]The arbitrary combinations of these representative candidate materials would ensure a systematic study of the SPR-TMD interaction process. Ultrafast pump-probe spectra together with steady-state absorption/luminescence spectra techniques revealed that, with the decoration of plasmonic metal nanoparticles, hot carriers were generated from the NPs and injected into the TMD monolayers. Instead of being immediately injected to the free carriers of the TMDs, the hot carriers will most likely interact with excitons in TMDs after the formation of excitons and introduce the formation of multi-interaction particles of trion and/or biexcitons under our experimental conditions.

2. Result and Discussion

2.1. Static Optical Characterization of MoX_2 Monolayers with Plasmonic Nanoparticles

Nanostructured plasmonic noble metals (namely, AgNPs/AuNPs) were deposited directly on single crystal MoX_2 monolayers via lift-off free PVD techniques (see Experimental Section and Figure S1, Supporting Information), to eliminate the nanoparticle nonuniformity, exclude the effects of surface contamination, and enable scalable nanoparticle deposition. **Figure 2**a shows the optical images of MoS_2 and its heterostructures with AgNPs and AuNPs, respectively. Distinct contrast under white light illumination can be observed between the pristine samples and the ones with NPs deposition, indicating drastic absorption variations due to plasmonic effects. As shown in the SEM images of Figure 2b,c and Figure S2 (Supporting Information), AgNPs and AuNPs with the size ranging from 5 to ≈30 nm were deposited both on the TMD monolayers and the blank substrate. It is noteworthy that the morphology between the two areas represents slight variation, with larger NPs observed on the TMDs region. This variation can be attributed to the surface property difference between TMDs and CaF_2 substrate as the NPs morphology

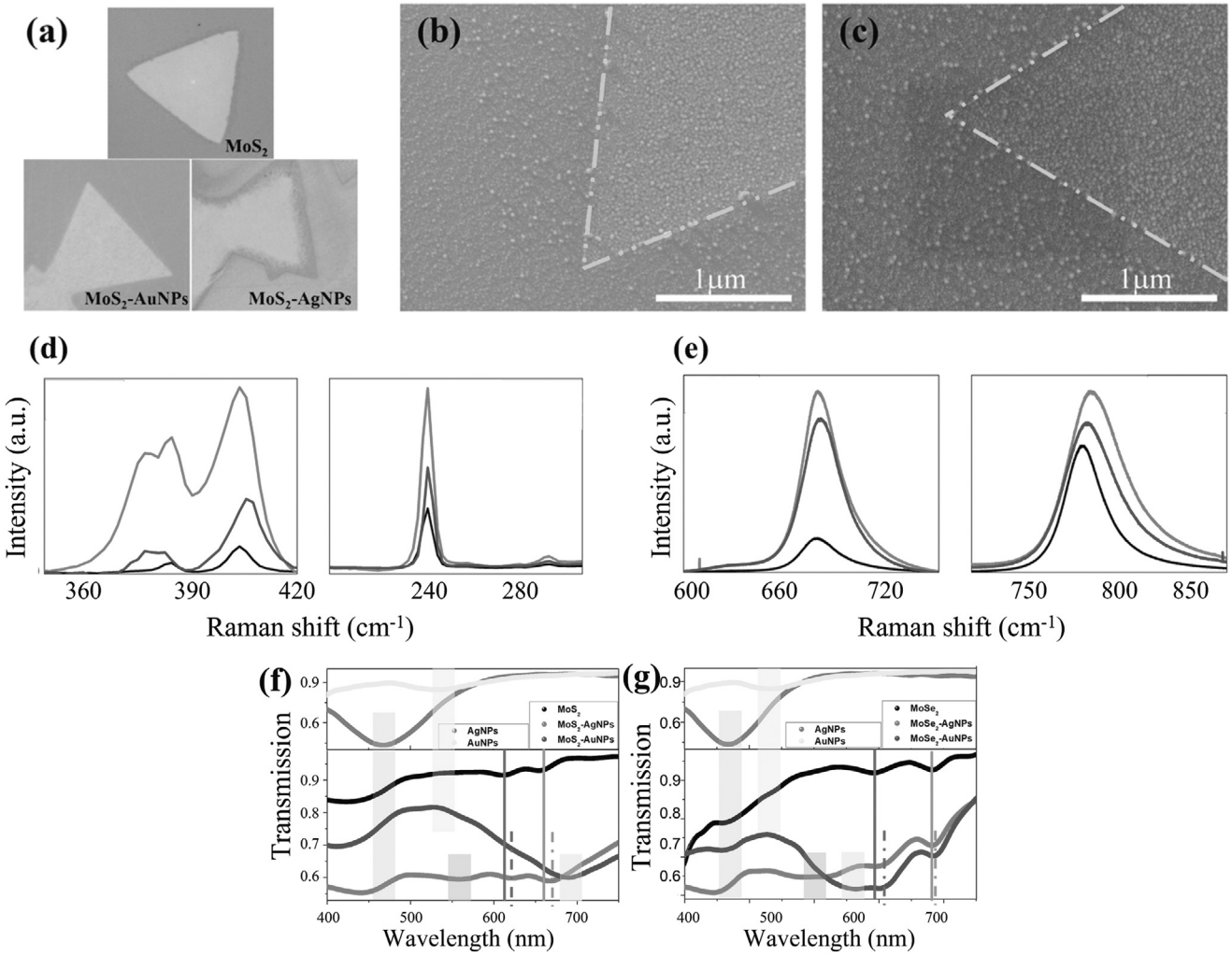

Figure 2. Characterizations of the plasmonic metal-semiconductor junctions. a) White light optical images of pristine MoS_2 and plasmonic metal nanoparticles decorated MoS_2 on CaF_2 substrate. b,c) SEM images of MoS_2-AgNPs (where NPs are nanoparticles) and MoS_2-AuNPs, respectively. The morphologies of NPs between the MoS_2 area and bare substrate area vary due to the difference in surface energy. Room temperature d) Raman and e) photoluminescence spectra of MoS_2 and $MoSe_2$ decorated with plasmonic metal nanoparticles represent different degree of local field enhancement and PL peak position shift. UV-Visible transmission spectra of the f) MoS_2-NPs and g) $MoSe_2$-NPs samples. Spectra from the metal nanoparticle area were illustrated for reference. The yellow boxes indicate the wavelength of surface plasmon resonances (SPRs) of Au NPs, and the gray boxes indicate the wavelength of SPRs of Ag NPs. With the decoration of NPs, the transmission is greatly reduced for both MoS_2 and $MoSe_2$, indicating strong photon absorption and scattering induced by the SPR from NPs. Both the exciton peaks of MoX_2 and the resonance peaks of NPs were red-shifted, suggesting strong interfacial interactions.

is surface energy sensitive.[29] The crystallinity of TMDs with the NPs decoration was verified by room temperature Raman spectra (Figure 2d). One can see from Figure 2d that fingerprint peaks of 2H phases were clearly present for the corresponding TMDs, excluding possible phase change upon metal deposition.[30] Both MoS_2 and $MoSe_2$ show Raman enhancement when covered by Ag/Au NPs with varying enhancement degrees. The Raman enhancement can be attributed to both local field enhancements and possible charge transfer processes.[31] Room temperature photoluminescence (Figure 2e) of the TMD-NPs represent intensity magnification and peak red shift with the deposition of plasmonic metals. The intensity magnification was mainly introduced by the local enhancement effects while peak red shift may be attributed to either plasmon-exciton interaction[32] or SP induced local electric field enhancement.[33] Comparison on the enhancement degree between the metal NPs revealed a higher enhancement degree of the AgNPs over AuNPs for both TMDs in either Raman or PL spectra, suggesting a higher local enhancement effect of the AgNPs (Figure S3, Supporting Information).

To further understand the SP resonance of the nanoparticles (NPs) and their interactions with TMDs, spatially resolved transmission spectra of the TMD-NPs were measured, using an inverted microscope and a monochromator. The spectra were plotted in Figure 2f,g and the corresponding mapping in certain peak wavelengths in Figure S4 (Supporting Information). As illustrated in Figure 2f,g, intrinsic SPR peaks of NPs were observed for both AgNPs (≈460 nm) and AuNPs (≈520 nm), agreeing with the NPs morphology characteristics in Figure 2b,c as both AgNPs and AuNPs exhibit highly

disordered profiles, with geometry configurations induced SP resonances prohibited. The TMD-NPs show remarkable absorption enhancement over the visible region, with the A and B excitonic absorption peaks observed for the pristine TMDs and TMD-NPs. The excitonic peaks indicate that the excitonic effects are still dominating in the TMDs with NPs decoration. Similar to the one in luminance spectra in Figure 2e, absorption peak positions of A and B excitons of TMDs were red shifted upon NPs deposition, indicating strong plasmon-exciton interactions.

With NPs successfully deposited on TMD monolayers, surface plasmon induced local field enhancement and plasmon-exciton interactions were verified via optical spectra. The nanoparticle decoration seems induce more remarkable spectrum enhancement in MoS_2-NPs over $MoSe_2$-NPs (Figure S3, Supporting Information), agreeing monotonically with the absorption enhancement (Figure S4, Supporting Information). However, SPR induced local field enhancement was reported to have significant influence on absorption/emission spectra, and their effects cannot be excluded from the room temperature characterizations. Low temperature PL measurements were therefore applied to quench and exclude the plasmonic field enhancement effects, and to better verify the plasmon-exciton interaction by distinguishing the PL contributions between the exciton and trion[34] (also refer to discussions in Figure S5, Supporting Information).

As illustrated in **Figure 3**a,b, the normalized PL spectra for MoS_2 and $MoSe_2$ vary with the illumination fluence, with an additional peak appear at a longer wavelength. Though emerged, peak fitting (Figure S6, Supporting Information) revealed a two-peak for both MoS_2 and $MoSe_2$, with peak energy splitting of 35 meV and 22 meV, respectively. The peak splitting agree with the energy difference between exciton and trion[35] for the two 2D semiconductors. Emission peaks with higher energy were assigned to exciton and the one with lower energy assigned to trion. With the decoration of NPs, the spectral distribution exhibit similar evolution for both MoS_2-NPs and $MoSe_2$-NPs, while the spectral weight varies with plasmonic metal NPs (Figure 3a,b). Spectral weight of trion was calculated as trion ratio: $R_{\text{Trion}} = A_{\text{Trion}}/(A_{\text{Trion}} + A_{\text{Exciton}})$, where A_{Trion} and A_{Exciton} are the peak areas for trion and exciton, respectively. The fluence dependence of trion ratio for the TMD-NPs were illustrated in Figure 3c,d, respectively. One can see from Figure 3c,d that the trion ratio was enhanced with the metal deposition under the same illumination laser intensity before saturation behavior emerge due to possible bi-exciton formation, suggesting a carrier doping process in TMD-NPs as the trion was reported to be originated from the interaction of exciton with external carriers and could be tuned by the carrier doping effects via electrostatic gate voltage or ionic liquid.[34] Given the hot-carrier generation nature of plasmonic NPs, it is reasonable to assume that the carrier doping effects in the TMD-NPs was introduced by the plasmonic hot carriers via carrier injection process. With the illumination of light, the plasmon generated at the metal NPs will be relaxed to hot carriers within tens of femtoseconds followed by high energy carriers injected into carrier acceptors (excitons in TMDs) by overcoming the energy barrier and be bounded by the exciton to form trion and possible high order quasi particles such as bi-excitons. However in our experiments, due to instrumental limitations such as temperature and wavelength resolution, we cannot effectively observe higher order effects, so we attribute the hot-carrier injected quasi particles to trion.

However, when examining the interaction efficiency between the hot carrier and excitons, it is surprising to notice that the AuNPs exhibit higher injection ratio than Ag NPs under the circumstances studied as the trion ratio are higher for both MoS_2-AuNPs and $MoSe_2$-AuNPs. The phenomenon agrees with the literatures as most of the SPR-TMDs based research highlighting the carrier's injection process are gold nanostructure based.[30,36–38] Considering that silver has a relatively stronger local enhancement to generate more hot carriers (Figure S3, Supporting Information) and higher Fermi level which can favor the injection process by lowering the Schottky barrier (Figure S7, Supporting Information), the higher injection efficiency of gold suggests us that the dynamic properties of the plasmonic hot carrier as well as the exciton formation kinetics may play critical roles for the interaction. Actually, gold normally possesses a longer hot carriers relaxation time (≈500 fs) than silver (≈350 fs),[19,39] better overlaps with the exciton formation duration for TMDs (≈400-800 fs).[18] Furthermore, the great fluence-dependence (Figure 3) and wavelength independence (Figure S8, Supporting Information, and Discussion therein) of TMD-NPs suggests an interesting dynamic interaction mechanism. It's been widely established that the plasmon thermal relaxation kinetics is illumination fluence dependent, high laser intensities can shorten the hot-carrier formation time and extend their cooling time, both favoring the carrier injection process dynamically.

2.2. Incoherent Relaxation Across the MoX_2-NPs Interface Before Exciton Formation

We then investigate the dynamical signature in SPR/TMD heterostructures on the exciton formation process and corresponding effects of plasmonic metals decoration, by applying spatially resolved visible pump/mid-infrared probe micro-spectroscopy. As schematically illustrated in **Figure 4**a, with pump photon excitation, free carriers in TMDs will be generated instantly and relaxed to form excitons, while the Mid-IR probe has smaller photon energy than the exciton binding energy of monolayer TMDs. So, the Mid-IR probe photons will be incapable to de-bind the as-formed excitons. Therefore, the waiting-time-dependent signals of the visible pump/ Mid- Infrared probe reflect the free carriers dynamic lifetime before exciton formation in TMDs, revealing the exciton formation time.[40,41] The pump photon energy is chosen to be 3.1 eV, while the probe energy is chosen to be 0.25 eV below all reported exciton binding energy in TMDs. The pump energy simulates the real-world scenario of SP enhanced TMD systems, which generate not only the SP in metal NPs, but also free carriers in TMDs.

From Figure 4b,e, we can see that both MoS_2 and $MoSe_2$ exhibit ultrafast kinetics of the photo-induced absorption from free carriers or weakly binding excitons with a lifetime of around 1 ps, indicating ultrafast free carrier relaxation processes to form excitons. With plasmonic NPs, corresponding dynamic signal intensities were enhanced for both TMDs,

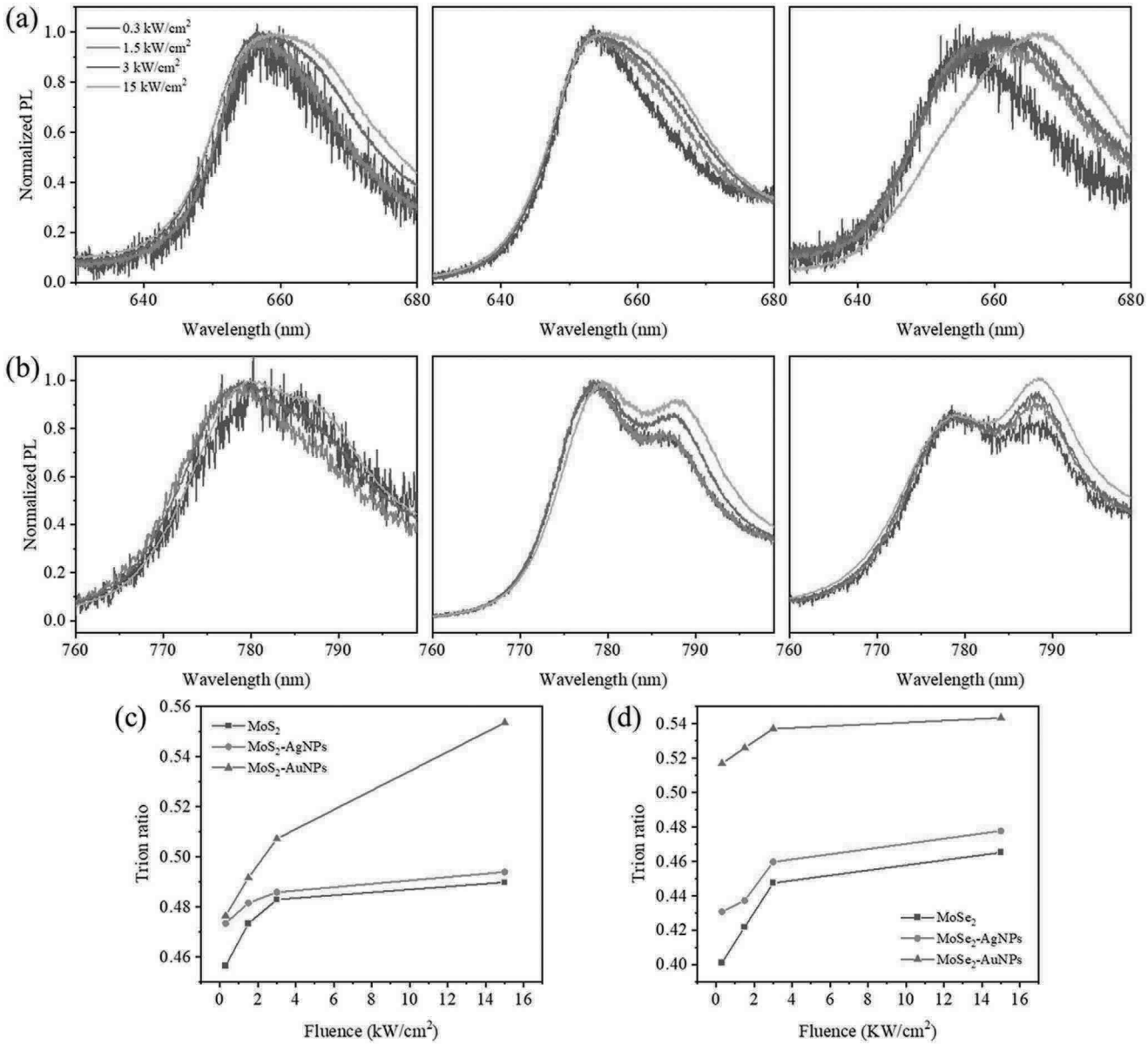

Figure 3. Exciton-trion spectral weight evolution in transition metal dichalcogenide (TMD) nanoparticles (NPs). a) Low temperature (80 K) PL characterizations of the MoS_2-NPs systems with different laser fluence under 532 nm laser. The PL intensity was normalized to the exciton peak intensity. b) Low temperature (80 K) PL characterizations of the $MoSe_2$-NPs systems. c) Trion ratio for the MoS_2-NPs system. With the decoration of NPs, the trion ratio of MoS_2 were enhanced while AuNPs induced higher trion ratio than Ag NPs. d) Trion ratio for $MoSe_2$-NPs under the same pump intensities. Similar phenomenon with the MoS_2-NPs was revealed for $MoSe_2$-NPs.

indicating a stronger response induced by local field enhancement while AgNPs for both TMDs produce larger enhancement effects than AuNPs. This instant enhancement and variable enhancement ratio agree with static optical characterizations, confirming the universal existence of local field enhancement. However, we were surprised to find out that normalized waiting-time-dependent dynamics in Figure 4c,f for both MoS_2 and $MoSe_2$, remain identical when undecorated or decorated with either AuNPs or AgNPs. And it is worth to mention that the AuNPs and AgNPs produce negligible visible pump/mid-IR probe signals, see Figure S13 (Supporting Information). Moreover, although the probe signal intensities increase linearly with pump fluence, the kinetics are invariant with fluence for MoS_2-NPs (Figure S10, Supporting Information) and $MoSe_2$-NPs (Figure S11, Supporting Information). Exponential fitting (Figure 4d,g) shows that the exciton formation time for MoS_2 with or without NPs are 0.6 ± 0.05 ps while the one for $MoSe_2$ are 1.1 ± 0.1 ps. These unexpected results reveal the irrelevance between the plasmonic evolution process and the free carrier relaxation process at the NPs-TMDs interface before the formation of exciton, suggesting that for both MoS_2 and $MoSe_2$, SP induced hot-carrier transfer do not happen before the formation of excitons. The hot carriers are known to be formed in a timescale of tens of fs, much faster than exciton formation in

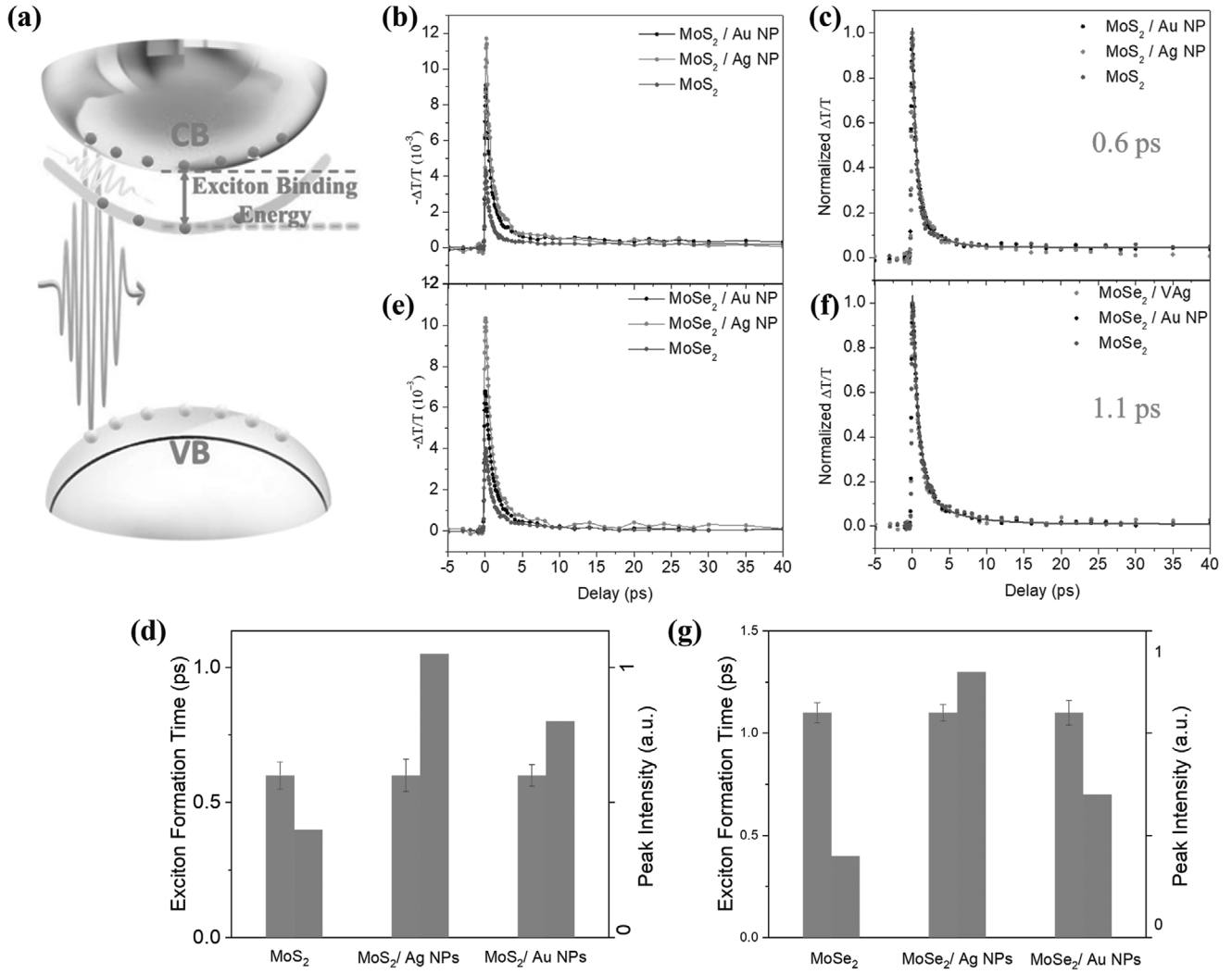

Figure 4. Waiting-time-dependent visible pump/mid-IR probe spectroscopies. a) Schematic illustration of physical processes in a photo excitation and detection of surface plasmon resonance (SPR)/transition metal dichalcogenide (TMD) system using visible pump mid-IR probe spectroscopy. The mid-IR probe (yellow) has an energy smaller than the TMD exciton binding energy, which is capable to detect the dynamic relaxation of pump (purple) excited electro-hole pairs. b) Absolute transient signal showing temporal evolution of transient absorption for MoS_2 and MoS_2-NPs (where NPs are nanoparticles). c) Normalized transient absorption signal of MoS_2 and MoS_2-NPs, presenting identical dynamic process among the samples. d) Exponential peak fitting output of the absolute transient absorption, with exciton formation time (light magenta) and absolute transient absorption signal (light gray) illustrated. e–g) Absolute, normalized, and exponential peak fitting of transient absorption for $MoSe_2$ and $MoSe_2$-NPs. Zoom-in of (c) and (f) is shown in Figure S9 (Supporting Information).

TMDs (hundreds of fs). For the SPR-TMDs, the local enhancement degree and Schottky barriers varied greatly among the TMD-NPs systems, it is thus expected that hot-carrier quantity, population, and lifetime will vary drastically upon light illumination. We postulate that if the charge transfer/interaction occurs during exciton formation process, the dynamic process would be altered resulting in a detectable signal with the mIR probe distinguishing between plasmonic metals, as mIR is sensitive to the transfer process while insensitive to the hot-carrier relaxation process.[6] However, due to the limitation of our instrument response function (IRF) of ≈100 fs, we cannot rule out the ultrafast hot-carrier injection pathways that are much faster than 100 fs by experiment.

The discovery can exclude possible pathways of direct hot-carrier generation in TMD conduction band in Figure 1b as the direct carrier generation will have significant impact on the free carrier kinetics of visible pump/ mid-infrared probe experiments. In fact, nonadiabetic molecular dynamics simulations combined with time-dependent density functional theory have revealed a traditional charge injection mechanism in Au nanorod-MoS_2 system, involving the rapid decay of plasmons into free electrons and subsequent charge injection.[42] The injection mechanism was attributed to the weak vdW Au-MoS_2 interface and the fully coordinated surface of MoS_2. The simulation principle and corresponding conclusions agree well with the mIR results, which could explain the uncorrelated relaxation process between plasmonic hot carriers and photonic free electron-hole carriers at the early stage. Nevertheless, it is not yet appropriate to draw a dynamic picture of the charge carrier-exciton interactions, considering the competition among

plasmonic carrier injection, possible energy transfer, and carrier recombination. To further explore the existence of hot-carrier transfer, we raise the probe photon energy to near-IR (nIR) to study the process after exciton formations. The near IR probe with energy of 1.53eV, which is larger than the exciton binding energy of TMDs while smaller than their band gap, has been extensively used to study the charge carrier injection process while measuring the exciton lifetime.[43–45]

2.3. Exciton-Formation-Triggered Hot-Carrier Injection

The transient absorption signal with near IR (1.53 eV) probe of pristine MoX_2 and NPs decorated MoX_2 are plotted in **Figure 5**a,b, respectively. The MoS_2 and $MoSe_2$ exhibit pure photo-induced absorption, which indicates an excitonic lifetime of a few ps. When decorated with metal NPs, two features emerge for both TMDs, i.e., a negative bleach signal in the very early waiting time and much longer exponential decay signal. The exponential decay signal reflected the quasi-particle lifetimes of the TMDs, while the bleach signal was from the electron–electron and electron–phonon scattering of SPs,[39] originates from either the interfacial charge injection process or plasmon delay in metal NPs. Bi-exponential fitting revealed much larger decay time constant for NPs decorated MoX_2, indicating extended particle lifetime induced by plasmonic NPs (Figure 5c). Comparisons between the MoS_2-AuNPs and MoS_2-AgNPs revealed that the particle lifetime for AuNPs injected MoS_2 are longer than MoS_2-AgNPs, which agree with the higher trion spectra ratio in Figure 3 as trion is a bounded state and has longer lifetime than exciton.

Pump fluence dependent experiments (Figure 5d and Figure S12, Supporting Information) for the TMD-NPs system were performed to distinguish the effects between charge injection and plasmon delay, as the lifetime of transient bleach for plasmon delay of standalone noble metal nanoparticles

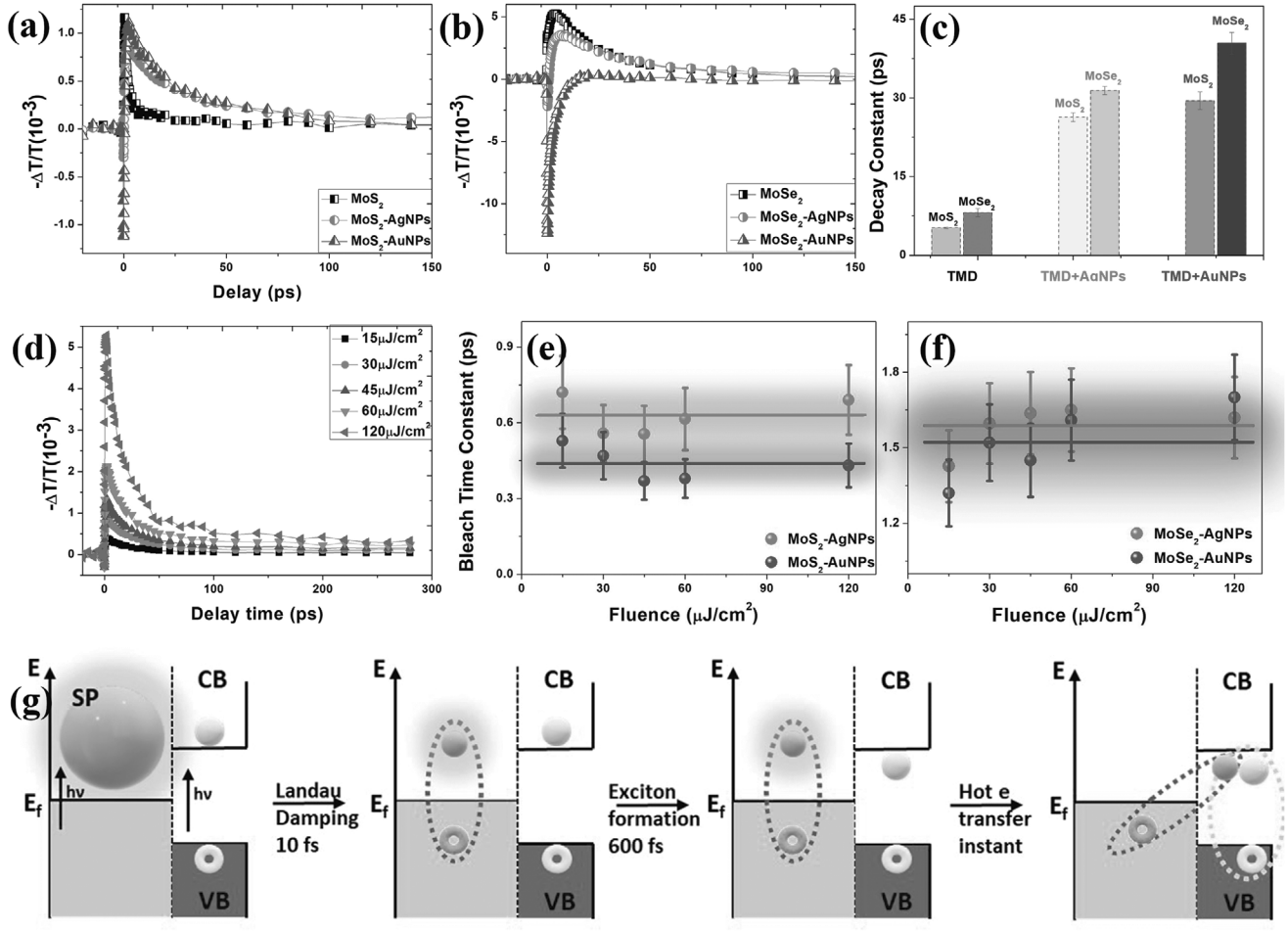

Figure 5. Temporal evolutions of visible pump/near-IR probe spectroscopies. a,b) Temporal evolution of transient absorption for MoS_2-NPs (where NPs are nanoparticles) and $MoSe_2$-NPs, respectively. Two features emerged with the NPs decoration. c) Decay constant from biexponential curve fitting of transient absorption for MoS_2-NPs and $MoSe_2$-NPs. The decay constant was largely extended with plasmonic NPs, agrees with the higher trion ratio induced by NPs decoration. d) Fluence dependent pump probe traces of MoS_2-AgNPs. e,f) Bleaching time constant with pump fluence for MoS_2-NPs and $MoSe_2$-NPs, respectively. Average and standard deviation of the bleach time constant over variable fluence were illustrated for reference. The time parameters were insensitive to pump fluence. g) Physical pathway of interfacial hot carrier injection to transition metal dichalcogenide (TMD) monolayers.

increases linearly with increasing pump fluence.[39] Fitting of corresponding spectrum considering IRF were performed on the basis of single exponential time constant of bleach (negative signal) and double exponential exciton lifetime (positive signal),[43] with the pump pulse temporal profile as ≈100 fs. Bleach time constant of TMD-NPs were extracted and plotted in Figure 5e,f, respectively. One sees that the bleach time constant for MoS_2-NPs are of 0.6 ± 0.2 ps, while 1.5 ± 0.2 ps for $MoSe_2$-NPs, which are independent within experimental accuracy. The independence of bleaching constant on pump fluence suggested that the observed bleaching signal originates from the hot-carrier injection process rather than decay of standalone SP induced hot carriers as the latter is highly fluence dependent.[39] And it is worth mentioning that the transient response can be altered by transient variation in dielectric permittivity of TMDs, however they normally emerge as bandgap renormalization effects which are outside our probe photon energies. It is noteworthy that the bleach time constant for MoS_2 and $MoSe_2$ with different metal NPs are close to their exciton formation time, indicating strong correlation between the charge carrier injection and the exciton formation.

3. Discussion

Based on the discussions above, the surface plasmon induced carrier injection pathway in SPR-TMDs can be illustrated schematically in Figure 5g (take the hot electron injection as an example). Initially, by photo-excitation, hot carriers in NPs and electron-hole pairs in MoS_2 were produced in less than a few tens of fs. The as-generated plasmonic hot carriers and the semiconducting electron-hole pairs then relax independently, with interfacial charge/energy transfer prohibited along the SPR-TMD interface. In ≈600 fs, the TMDs' excited e-h pairs form excitons followed by instant (quicker than our instrumental response) hot carriers (hot electrons or hot holes) transfer to MoS_2 atomic layer. The as-injected hot carriers were thus captured by the excitons to form bounded states (trions), which have lower energy and extended lifetime. With illumination fluence increases, the production ratio of hot carriers surpasses those of TMD excitons, inducing fluence dependence of trion ratio increment and saturation.

The pathway revealed here differed from either the traditional hot-carrier injection mechanism (Figure 1a) or the direct hot-carrier generation mechanism between coherent interfaces (Figure 1b). In all models, timescale plays fundamental role in determining the hot carrier's distribution along the interface and thus their probability of interacting with nearby acceptor via either injection or direct generation, while the mechanism proposed here highlighted kinetics matching between the SPR and TMDs as TMD exciton formation timescale plays determinant role for the interfacial carrier transfer. However, it should be noted that possible hot-carrier injection pathways without exciton formation is still possible but outside our experimental observations. As the exciton formation time in TMD monolayers are in the range of 500 fs–1 ps, slower than that of hot-carrier formation (≈tens of fs), it is possible to enhance the injection efficiency by metal-TMD covalent bonding,[45] slowing the hot carriers e-e or e-p relaxation time via either optimizing plasmonic nanostructure morphology, composition and dielectric environment,[46] or increasing phonon intensity.[47] The hypothesis was proved to be efficient in the trion ratio enhancement in Figure 3. On the other hand, for circumstances aiming at ultrafast opto-electrical response of TMDs where hot carrier or trion may present negative influence,[48] perspectives of limiting the hot-carrier injection/trion formation might be realized by mismatching the dynamics process across the interface layer as the injection dynamics is dominated by the exciton formation process. Furthermore, given the fact that interlayer exciton formation in TMD heterostructures is much faster (with formation time of ≈100 fs), and is a better match with the plasmonic hot-carrier formation time, it's reasonable to predict that the plasmonic charge carrier injection process would be more efficient.[40,49]

Along with the plasmonic local field enhancement, understanding and controllable manipulating the carrier injection in SPR-TMDs are of essential importance for TMDs related practical applications upon light-matter interaction, giving the fact that the carrier injection process will greatly enhance the trion ratio (Figure 3). The trion, which have large binding energies and display valley-selective properties that are similar to those of the neutral excitons, were believed to present similar optical performance as excitons.[50] Intuitively, the greatly extended quasiparticle lifetime observed in Figure 5g is critical for TMD based photovoltaics and photocatalyst devices' performance enhancement. In contrast to neutral excitons, the charged nature of the trion (charged exciton with positive/ negative charge) enable further particle guidance with applied electric and/or magnetic field, and suggest schemes to overcome the losses associated with exciton diffusion and to efficiently collect the photogenerated current.[51] Trion in TMD monolayers have been reported to find applications in second harmonic generation, valleytronics, optical information storage, and quantum hall effects,[38,52–54] all of which may be further investigated via SPR-TMD approach by manipulating the hot-carrier injection process.

4. Conclusions

We demonstrated the ultrafast hot-carrier interaction pathway between the plasmonic nanoparticles and the transition metal dichalcogenide monolayers. Upon optical excitation, we characterized both steady-state and dynamic exciton evolution in MoX_2 monolayer induced by plasmonic NPs decoration. Our study found that with plasmonic AgNPs and AuNPs decoration, the TMD trion ratio was greatly enhanced attributing to hot-carrier injection effects while AuNPs presented higher injection efficiency. Kinetics examination revealed an exciton formation triggered hot-carrier injection mechanism across the MoX_2-NPs interface, with the as-injected hot carriers captured by excitons to form trions. The better overlapping of AuNPs' hot-carrier lifetime with TMD exciton formation timescale enables higher injection efficiency, while higher injection ratio will result in extended lifetime of bounded particles. The dynamic pathway revealed here highlights the fundamental role of TMD exciton kinetics in plasmonic metal-TMD interaction, opens new opportunities for controllable manipulation of hot-carrier

injection process, and inspires future research toward opto-electrical device design with light-matter interaction.

5. Experimental Section

MoX_2-Ag/AuNPs Sample Fabrication: To fabricate the samples, CVD grown MoX_2 monolayers were first transferred to CaF_2 substrates for transmission mode laser experiments. The MoX_2 triangles on the CaF_2 substrate were confirmed by optical microscope, followed by vacuum annealing at 300 °C for 2 h.

The samples were then loaded in an ultrahigh vacuum chamber (10^{-7} Torr) to deposit 3 nm Au film via e-beam evaporation at a rate of 0.1 Å s^{-1}. During the evaporation, the samples were half exposed to gold vapor by a shadow mask. The as-deposited sample was then annealed under flowing Ar_2 at 400 °C for 2 h to generate gold nanoparticles. The samples were then deposited by silver nanoparticles via oblique angle deposition in the same e-beam evaporation system at room temperature. Before AgNPs deposition, the sample was firstly self-rotated by 90° to get half-exposed followed by tilting the samples by 88°. The deposition rate was 5 Å s^{-1}.

The morphology of as deposited nanoparticles was characterized in an environmental field-emission SEM (FEI Quanta 400 ESEM FEG) under low vacuum mode.

Steady State Optical Characterizations: Raman and PL spectroscopy were carried out using a Renishaw InVia Raman microscope. The excitation light is a 532 nm laser, with an estimated laser spot size of 1 µm and maximum laser power of 1 mW. Before test, the samples were loaded into a vacuum chamber with cooling stage within Ar_2-filled glove box. For room temperature and low temperature test, the stage temperature was cooled by flowing liquid nitrogen and temperature controlled by a feedback system with the thermometer reading as 300 and 80 K, respectively.

UV-Vis transmission spectra and corresponding mapping of MoX_2-NPs were collected between wavelengths of 300 to 900 nm on a homemade setup. The spectra resolution is of 1 nm with spatial resolution of 5×5 µm.

Ultrafast Visible-NIR/Infrared Micro-Spectroscopy: The experimental setup of the ultrafast visible-NIR/infrared micro-spectroscopy is from our previous publications.[26–27] Briefly, the output of a femtosecond amplifier laser system (at a repetition rate of 1 kHz, 1.6 mJ energy per pulse, 800 nm central wavelength, and a pulse duration of ≈40 fs, Uptek Solutions Inc.) is split into two parts. One is used to pump a home-built nonlinear optical parametric amplifier to generate visible and near-IR-1 laser pulses with tunable wavelengths, and the other is directed to generate an ultra-broadband super-continuum pulse, which covers almost the whole mid-IR region or a near-IR-2 pulse. In ultrafast experiments, the visible or NIR-1 pulse is the pump light with the central wavelength and excitation power adjusted based on need. The interaction spot on the samples varies from 120 to 250 micron. The mid-IR super-continuum pulse or NIR-2 pulse acts as the probe light, which is focused at the sample by the reflective objective lens (15X/0.28NA, Edmund Optics Inc.) to reduce the spot size to the level of the sample area (<40 µm). A 300-megapixel microscope digital camera is used to align the pump/probe beam to proper sample area. The probe light is detected by a liquid-nitrogen-cooled mercury-cadmium-telluride (MCT) array detector or InSb detector after frequency resolved by a spectrograph with a resolution of 1–3 $cm^{-1,}$ which is dependent on the central frequency. The time delay between the pump light and probe light is controlled by a motorized delay stage.

Supporting Information

Supporting Information is available from the Wiley Online Library or from the author.

Acknowledgements

This work was supported by the Welch Foundation grant C-1716, and the NSF I/UCRC Center for Atomically Thin Multifunctional Coatings (ATOMIC) under award # IIP-1539999. This research made use of instruments in the Shared Equipment Authority at Rice University. The authors thank for the useful discussions with Prof. Peter Nordlander, Prof. Junichiro Kono, Prof. Zhengjun Zhang, and Dr. Yu Huang.

Conflict of Interest

The authors declare no conflict of interest.

Author Contributions

X.W. and W.W. contributed equally to this work, they designed and performed the experiments, analyzed data, and wrote the manuscript. P.M.A., J.L., and W.W. conceived the idea, revised the manuscript and led the project. X.Z., S.J., Y.G., and W.C. supplied the TMD monolayer samples. H.C., H.Z., and J.Z. contributed to the pump-probe spectroscopy test.

Data Availability Statement

The data that support the findings of this study are available from the corresponding author upon reasonable request.

Keywords

2D materials, plasmonics, ultrafast spectroscopy, hot electrons, excitons

Received: January 12, 2021
Revised: November 8, 2021
Published online:

[1] H. A. Atwater, A. Polman, *Nat. Mater.* **2010**, *9*, 205.
[2] S. Linic, P. Christopher, D. B. Ingram, *Nat. Mater.* **2011**, *10*, 911.
[3] M. L. Brongersma, N. J. Halas, P. Nordlander, *Nat. Nanotechnol.* **2015**, *10*, 25.
[4] P. Törmä, W. L. Barnes, *Rep. Prog. Phys.* **2014**, *78*, 013901.
[5] M. W. Knight, H. Sobhani, P. Nordlander, N. J. Halas, *Science* **2011**, *332*, 702.
[6] K. Wu, J. Chen, J. R. McBride, T. Lian, *Science* **2015**, *349*, 632.
[7] S. Tan, A. Argondizzo, J. Ren, L. Liu, J. Zhao, H. Petek, *Nat. Photonics* **2017**, *11*, 806.
[8] J. Miao, W. Hu, Y. Jing, W. Luo, L. Liao, A. Pan, S. Wu, J. Cheng, X. Chen, W. J. S. Lu, *Small* **2015**, *11*, 2392.
[9] W. Wang, A. Klots, D. Prasai, Y. Yang, K. I. Bolotin, J. Valentine, *Nano Lett.* **2015**, *15*, 7440.
[10] X. Yang, W. Liu, M. Xiong, Y. Zhang, T. Liang, J. Yang, M. Xu, J. Ye, H. Chen, *J. Mater. Chem. A* **2014**, *2*, 14798.
[11] Z. Yin, B. Chen, M. Bosman, X. Cao, J. Chen, B. Zheng, H. J. S. Zhang, *Small* **2014**, *10*, 3537.
[12] J. Xu, C. Li, H. Si, X. Zhao, L. Wang, S. Jiang, D. Wei, J. Yu, X. Xiu, C. Zhang, *Opt. Express* **2018**, *26*, 21546.
[13] E. Cao, W. Lin, M. Sun, W. Liang, Y. J. N. Song, *Nanophotonics* **2018**, *7*, 145.
[14] X. Li, J. Zhu, B. Wei, *Chem. Soc. Rev.* **2016**, *45*, 3145.

[15] Y. Liu, J. Guo, E. Zhu, L. Liao, S.-J. Lee, M. Ding, I. Shakir, V. Gambin, Y. Huang, X. Duan, *Nature* **2018**, *557*, 696.
[16] Y. Pan, S. Li, M. Ye, R. Quhe, Z. Song, Y. Wang, J. Zheng, F. Pan, W. Guo, J. Yang, *J. Phys. Chem. C* **2016**, *120*, 13063.
[17] K. F. Mak, J. Shan, *Nat. Photonics* **2016**, *10*, 216.
[18] P. Steinleitner, P. Merkl, P. Nagler, J. Mornhinweg, C. Schüller, T. Korn, A. Chernikov, R. Huber, *Nano Lett.* **2017**, *17*, 1455.
[19] Y. Zhang, S. He, W. Guo, Y. Hu, J. Huang, J. R. Mulcahy, W. D. Wei, *Chem. Rev.* **2017**, *118*, 2927.
[20] J. Madéo, M. K. Man, C. Sahoo, M. Campbell, V. Pareek, E. L. Wong, A. Al-Mahboob, N. S. Chan, A. Karmakar, B. M. K. Mariserla, *Science* **2020**, *370*, 1199.
[21] Y. Li, W. Liu, Y. Wang, Z. Xue, Y.-C. Leng, A. Hu, H. Yang, P.-H. Tan, Y. Liu, H. Misawa, *Nano Lett.* **2020**, *20*, 3747.
[22] H. Petek, *J. Chem. Phys.* **2012**, *137*, 091704.
[23] Y. Li, J. Shi, Y. Mi, X. Sui, H. Xu, X. J. J. o. M. C. C. Liu, *J. Mater. Chem. C* **2019**, *7*, 4304.
[24] J. Shah, *Ultrafast Spectroscopy of Semiconductors and Semiconductor Nanostructures*, Vol. *115*, Springer Science & Business Media, Berlin **2013**.
[25] C. Jin, E. Y. Ma, O. Karni, E. C. Regan, F. Wang, T. F. Heinz, *Nat. Nanotechnol.* **2018**, *13*, 994.
[26] W. Du, J. Zhao, W. Zhao, S. Zhang, H. Xu, Q. Xiong, *ACS Photonics* **2019**, *6*, 2832.
[27] A. Camellini, A. Mazzanti, C. Mennucci, C. Martella, A. Lamperti, A. Molle, F. B. d. Mongeot, G. D. Valle, M. Zavelani-Rossi, *Adv. Opt. Mater.* **2020**, *8*, 2000653.
[28] H. Shan, Y. Yu, X. Wang, Y. Luo, S. Zu, B. Du, T. Han, B. Li, Y. Li, J. Wu, F. Lin, K. Shi, B. K. Tay, Z. Liu, X. Zhu, Z. Fang, *Light: Sci. Appl.* **2019**, *8*, 9.
[29] V. F. Puntes, K. M. Krishnan, A. P. Alivisatos, *Science* **2001**, *291*, 2115.
[30] Y. Kang, S. Najmaei, Z. Liu, Y. Bao, Y. Wang, X. Zhu, N. J. Halas, P. Nordlander, P. M. Ajayan, J. Lou, *Adv. Mater.* **2014**, *26*, 6467.
[31] Y. Deng, M. Chen, J. Zhang, Z. Wang, W. Huang, Y. Zhao, J. P. Nshimiyimana, X. Hu, X. Chi, G. Hou, *Nano Res.* **2016**, *9*, 1682.
[32] W. Liu, B. Lee, C. H. Naylor, H.-S. Ee, J. Park, A. T. C. Johnson, R. Agarwal, *Nano Lett.* **2016**, *16*, 1262.
[33] S. Najmaei, A. Mlayah, A. Arbouet, C. Girard, J. Léotin, J. Lou, *ACS Nano* **2014**, *8*, 12682.
[34] J. S. Ross, S. Wu, H. Yu, N. J. Ghimire, A. M. Jones, G. Aivazian, J. Yan, D. G. Mandrus, D. Xiao, W. Yao, *Nat. Commun.* **2013**, *4*, 1474.
[35] K. F. Mak, K. He, C. Lee, G. H. Lee, J. Hone, T. F. Heinz, J. Shan, *Nat. Mater.* **2013**, *12*, 207.
[36] Y. Shi, J. Wang, C. Wang, T.-T. Zhai, W.-J. Bao, J.-J. Xu, X.-H. Xia, H.-Y. Chen, *J. Am. Chem. Soc.* **2015**, *137*, 7365.
[37] W. Wang, A. Klots, D. Prasai, Y. Yang, K. I. Bolotin, J. Valentine, *Nano Lett.* **2015**, *15*, 7440.
[38] X. Wen, W. Xu, W. Zhao, J. B. Khurgin, Q. Xiong, *Nano Lett.* **2018**, *18*, 1686.
[39] G. V. Hartland, *Chem. Rev.* **2011**, *111*, 3858.
[40] H. Chen, X. Wen, J. Zhang, T. Wu, Y. Gong, X. Zhang, J. Yuan, C. Yi, J. Lou, P. M. Ajayan, W. Zhuang, G. Zhang, J. Zheng, *Nat. Commun.* **2016**, *7*, 12512.
[41] X. Wen, H. Chen, T. Wu, Z. Yu, Q. Yang, J. Deng, Z. Liu, X. Guo, J. Guan, X. Zhang, *Nat. Commun.* **2018**, *9*, 1859.
[42] Z. Zhang, L. Liu, W.-H. Fang, R. Long, M. V. Tokina, O. V. Prezhdo, *Chem* **2018**, *4*, 1112.
[43] X. Hong, J. Kim, S.-F. Shi, Y. Zhang, C. Jin, Y. Sun, S. Tongay, J. Wu, Y. Zhang, F. Wang, *Nat. Nanotechnol.* **2014**, *9*, 682.
[44] L. Yuan, T.-F. Chung, A. Kuc, Y. Wan, Y. Xu, Y. P. Chen, T. Heine, L. Huang, *Sci. Adv.* **2018**, *4*, e1700324.
[45] J. R. Dunklin, A. H. Rose, H. Y. Zhang, E. M. Miller, J. Lagemaat, *ACS Photonics* **2020**, *7*, 197.
[46] P. Christopher, M. Moskovits, *Annu. Rev. Phys. Chem.* **2017**, *68*, 379.
[47] R. L. Gieseking, M. A. Ratner, G. C. Schatz, *Frontiers of Plasmon Enhanced Spectroscopy*, Vol. *1*, American Chemical Society, Washington DC **2016**, pp. 1–22, Ch. 1.
[48] C. Lui, A. Frenzel, D. Pilon, Y.-H. Lee, X. Ling, G. Akselrod, J. Kong, N. Gedik, *Phys. Rev. Lett.* **2014**, *113*, 166801.
[49] K. F. Mak, J. Shan, *Nat. Nanotechnol.* **2018**, *13*, 974.
[50] F. Xia, H. Wang, D. Xiao, M. Dubey, A. Ramasubramaniam, *Nat. Photonics* **2014**, *8*, 899.
[51] D. Sanvitto, F. Pulizzi, A. J. Shields, P. C. M. Christianen, S. N. Holmes, M. Y. Simmons, D. A. Ritchie, J. C. Maan, M. Pepper, *Science* **2001**, *294*, 837.
[52] H. Yu, X. Cui, X. Xu, W. Yao, *Natl. Sci. Rev.* **2015**, *2*, 57.
[53] L. Langer, S. V. Poltavtsev, I. A. Yugova, M. Salewski, D. R. Yakovlev, G. Karczewski, T. Wojtowicz, I. A. Akimov, M. Bayer, *Nat. Photonics* **2014**, *8*, 851.
[54] M. Onga, Y. Zhang, T. Ideue, Y. Iwasa, *Nat. Mater.* **2017**, *16*, 1193.

